

Observation of a Bulklike Fermi Surface for a Monolayer of Ni on Cu(001)

G. J. Mankey,* K. Subramanian, R. L. Stockbauer, and R. L. Kurtz

Department of Physics and Astronomy, Louisiana State University, Baton Rouge, Louisiana 70803

(Received 19 August 1996)

We find that the photoelectron angular distributions from the Fermi surface of a monolayer Ni film on Cu are identical to those from thick Ni films and single-crystal Ni(001), and agree well with theoretical predictions for bulk Ni. This bulklike behavior in the monolayer film is attributed to the short screening length of electrons in metals, the similarity of the Ni and Cu cores, and a hybridization between Ni and Cu facilitating an interaction with the underlying crystal field. [S0031-9007(96)02282-X]

PACS numbers: 75.70.-i, 71.18.+y, 73.20.Dx, 79.60.-i

Multilayer structures consisting of ultrathin metal-on-metal layers exhibit unique properties derived from their unusual electronic structure such as quantum-well states [1], oscillatory magnetic coupling [2], and oscillatory superlattice conductivity [3]. The origin of these phenomena is related to properties of the interface and localization or confinement of the electron density within the layers. The electronic structure of the film and the interface can be investigated with photoemission.

For an isolated monolayer there is no periodicity in the normal direction and dispersion is confined within the plane of the film. This two-dimensional behavior is exhibited in many layered systems such as Ag/Cu(001) where 5 ML of Ag is required to establish bulklike behavior [4]. Theoretical calculations for isolated layers of Ni(001) show that the electronic structure of a single layer is very different from the bulk, with a reduced bandwidth and markedly different density of states [5,6]. Experimentally, however, the monolayer films must be deposited on a supporting substrate which may perturb the electronic structure.

Thin film electronic states will resemble those calculated for an isolated layer if the electron wave functions are localized within the film. For simple systems exhibiting pseudomorphic growth, such as the one presented here, the penetration of the electron wave function into the substrate can be estimated by assuming a simple rectangular potential barrier at the film/substrate interface [7]. For $3d$ electrons at the Ni/Cu interface the potential energy difference roughly corresponds to the band mismatch of about 2 eV, yielding a penetration of less than an angstrom. However, the calculations of Wang *et al.* predict a charge transfer from the Cu substrate into the Ni film [5]. This charge transfer acts to smooth out the potential barrier, allowing a larger penetration of the film electron wave functions and subsequent hybridization with the substrate electronic states.

A localization of electrons can give rise to a two-dimensional electronic structure, which is a unique property of surfaces, interfaces, and films. These two-dimensional states disperse within the plane of the surface or film, but do *not* disperse in the perpendicular direction. In contrast with this behavior, we find that atomically

thin Ni films on Cu(001) exhibit photoelectron emission patterns that do disperse strongly in the perpendicular direction and are consistent with a bulklike electronic structure within the monolayer.

The experiments were performed at the Center for Advanced Microstructures and Devices (CAMD) synchrotron facility. The Cu substrate was prepared using standard procedures [8]. Photoemission measurements were performed with a display-type ellipsoidal mirror analyzer which is described in detail elsewhere [9]. This instrument images the angular distributions of photoelectrons within a narrow energy range which, for the measurements described here, was selected to be the Fermi energy. Energy distribution curves of photoelectrons are obtained by integrating the emission over a 32° half-angle cone.

Since an accurate measure of film thickness and morphology is required to determine the two-dimensional character of the films, several techniques were used to independently establish growth characteristics. The films were deposited on a room temperature substrate, which is the optimum growth temperature for smooth films with an atomically sharp interface [10]. From a combination of x-ray photoelectron diffraction (forward scattering) measurements, $3p$ core-level intensity studies, and magnetometry using magnetic linear dichroism, we estimate our film thicknesses to be accurate within 25% [11]. In addition, the observation of sharp photoelectron angular distributions indicate that the films are well ordered. These observations are consistent with a recent STM study which indicates that there is no significant interdiffusion or three-dimensional clustering in the films [10]. The forward scattering measurements also confirm a good layer-by-layer growth mode [12].

Angle-integrated energy distribution curves from the 1.2 and 6 ML Ni/Cu(001) are shown in Fig. 1. For the 6 ML film, the spectra resemble bulk Ni, with only a weak feature below -2 eV due to emission from the Cu $3d$ band. The nearly complete attenuation of the Cu $3d$ band confirms that the substrate is covered by the Ni, and that there is little or no intermixing between Cu and Ni, nor is there any Cu segregating to the surface. At 1.2 ML of Ni, emission from the Ni $3d$ band is about half that of the $3d$ band of the substrate, consistent with a mean free path for

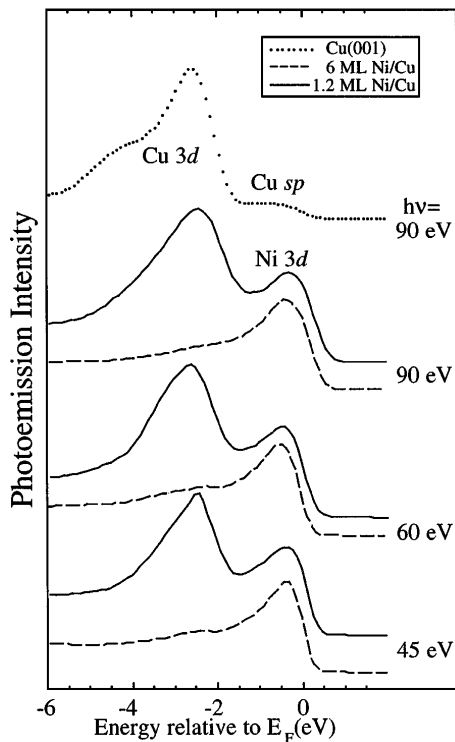


FIG. 1. Angle-integrated photoelectron energy distribution curves for pure Cu(001) at $h\nu = 90$ eV, and 1.2 and 6 ML Ni/Cu(001) films for photon energies of 45, 60, and 90 eV. Emission from Ni 3*d* electronic states is seen as a broad peak at the Fermi energy whereas the Cu 3*d* emission is seen 2 eV below E_F .

photoelectrons of about 3 ML. The attenuation of the Cu 3*p* core levels also suggests uniform growth with little or no intermixing. The line shapes for the Ni 3*d* peak in the two films, shown in Fig. 1, are almost identical, indicating that there is no significant narrowing of the bandwidth.

The dispersion of these bands can be monitored by collecting photoelectron angular distributions and monitoring their variation with photon energy (i.e., k_{\perp}). With a display analyzer, one observes an intensity map k_{\parallel} of a constant energy surface whose k_{\perp} location depends on photon energy. The images in Fig. 2 show the photoelectron angular distributions from the Fermi level for photon energies of 45, 60, and 90 eV. Figure 2(a) shows the patterns obtained from clean Cu(001), while Figs. 2(b) and 2(c) show those from a 1.2 and a 6 ML Ni film on Cu(001). The Cu(001) crystal was oriented with the [100] direction horizontal and with *p*-polarized radiation incident in the horizontal plane at 45° to the normal; along $[10\bar{1}]$. In (d) similar data are shown for single-crystal Ni(001); however, the [100] direction of the 45 and 60 eV images is $\sim 15^\circ$ from the horizontal. The three photon energies probe points in reciprocal space on a spherical shell that passes near the Γ point in the center of the 45 eV image, near the *K* and *X* points near the edges of the 60 eV images, and near the zone boundary *X* in the center of the 90 eV image.

The data in Figs. 2(a)–2(d) have been corrected only for channel plate efficiency and are plotted on a linear

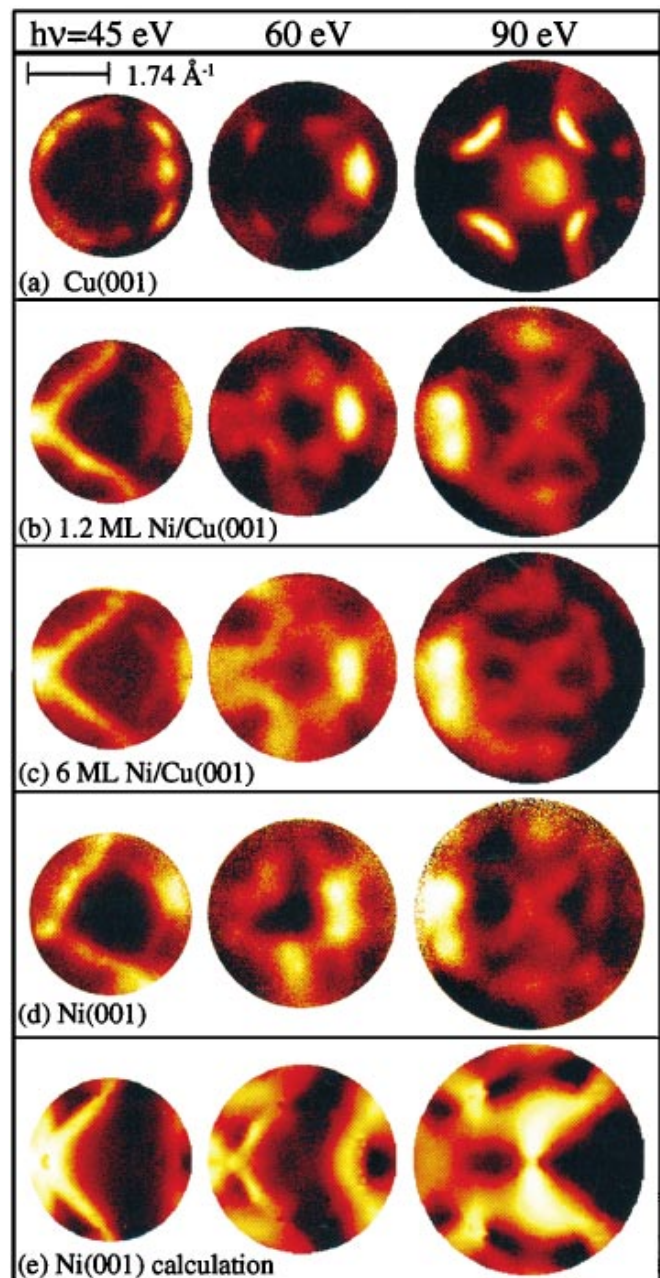


FIG. 2(color). Angular distributions of photoelectrons originating from the Fermi energy as a function of photon energy for (a) single-crystal Cu(001), (b) a 1.2 ML Ni film on Cu(001), (c) a 6 ML Ni film, and (d) single-crystal Ni(001). The images have been scaled to be linear in k_{\parallel} . (e) Calculations of the angular distributions of photoelectrons from bulk Ni(001).

intensity scale. The images have been scaled such that they are linear in parallel momentum and the photoemission intensity is maximum for the brightest feature and minimum for the darkest feature. The images exhibit a twofold rather than the fourfold symmetry of the substrate since the plane polarized nature of the incident photons produces a left-right asymmetry with respect to the (010) mirror plane. Any top-bottom asymmetry (except that mentioned for 2(d)) is due to a slight misalignment of the

crystal with respect to the plane of incidence or to minor distortions inherent in the optics.

In the center of 90 eV image of Fig. 2(a), one can see the spherical “body” of the Cu(001) Fermi surface. This is connected with “necks” along the [110] azimuths to four additional arcs which are the FS bodies from neighboring Brillouin zones. At 60 and 45 eV, the images probe that central Cu FS body with cross sections closer to the center of the zone. The most intense feature in the 60 eV image is an enhancement of intensity due to multiple-scattering.

When Ni is deposited, the FS cross sections change dramatically. By 1.2 ML, we no longer see any Cu-related features due to the very high Ni Fermi surface density of states and, in part, to the attenuation of Cu photoelectrons by the overlayer. The images from 1.2 and 6 ML Ni are essentially identical. For thicker films, distinct angular distributions are lost, consistent with a surface roughening reported previously [10].

The most striking feature of the data in Fig. 2 is the similarity of the patterns for the 1.2 and 6 ML films. In addition, these images are essentially identical to those obtained from the bulk single-crystal Ni(001) shown in Fig. 2(d). None of the features in Figs. 2(b) and 2(c) can be attributed to interface states since they are all observed at the same photon energies in photoemission from *bulk* Ni(001). Moreover, none of these features are surface states, since they are also seen in the same locations of the Brillouin zone of *bulk* Cu(001) at $E_F - 2$ eV, where similar *3d* initial-state bands are found.

In order to extract the orbital character and symmetry of the initial states, the photoelectron angular distributions were simulated using a second principles parameterized *bulk* ferromagnetic Ni band structure [13]. The band structure was determined by the diagonalization of a 21×21 Hamiltonian matrix for each spin. The angle-dependent photoemission matrix elements were then calculated from the analytical derivatives of the Hamiltonian with an artificial suppression factor for the component of incident radiation polarized perpendicular to the surface. Broadening of the angular distributions was simulated using an energy and group velocity dependent photoemission linewidth [14] convoluted with an instrumental broadening of 0.2 eV. All of the main features of the experimental images are reproduced by the calculation, as shown in Fig. 2(d). The relative intensities of the features are not as well reproduced at the highest photon energy most likely due to multiple-scattering [15].

Comparison of the polarization-dependent data with the computations of intensity asymmetry allows one to establish the orbital symmetry of the initial states. Initial states exhibiting left-right asymmetry, brighter on the left, have d_{xz} or d_{yz} orbital character. Initial states with no left-right asymmetry have d_{xy} orbital character. The absence of emission in the [100] azimuth and the presence of a vertical bar in the [010] is characteristic of a $d_{x^2-y^2}$ orbital. Bright emission only in the right half of the image

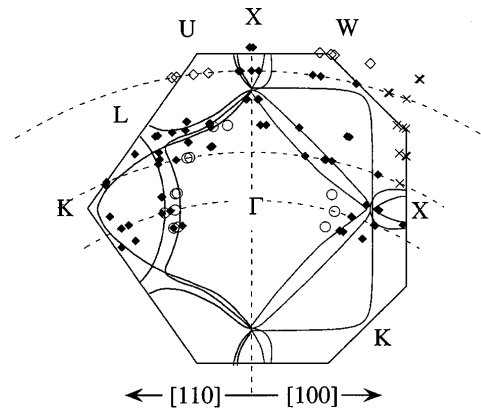


FIG. 3. Fermi surface contours for the 1.2 ML Ni film. The dashed arcs show the part of the Brillouin zone being probed by the three different photon energies of Fig. 2. The arc lengths indicate the acceptance angle of the analyzer. The filled diamonds represent *3d* band crossings, the open circles represent *sp*-like states. The crosses represent dispersionless features near the zone edge. The solid lines represent Fermi surface contours from a first-principles calculation by Wang and Callaway [16].

originates from initial states having a d_{z^2} or *sp* orbital character.

At 45 eV photon energy, d_{xz} and d_{yz} emission from both the majority and minority spin subbands is seen as bright diagonal lines on the left side of the image. The two bright diagonal lines are half of a diamondlike structure with the right half suppressed due to polarization selection rules. On rotating the sample azimuth by 45° , emission from these states forms a boxlike structure, preserving the left-right asymmetry. Emission from the *sp*- d_{z^2} hybrid band is seen as a faint circular arc on the right side of the $h\nu = 45$ eV images. However, the intensity of this feature is greater than that predicted by our calculation. The separate spin-up and spin-down subbands are not distinguishable in the data or the calculations for the 45 and 60 eV electron images due to the finite photoemission linewidth and experimental resolution. At 60 eV photon energy, the diagonal features on the left and the arc on the right have moved inwards, which are both clear indications of perpendicular dispersion. At 90 eV photon energy, the d_{xz} and d_{yz} bands have negligible photoemission matrix elements and the *sp*- d_{z^2} band has dispersed above the Fermi energy, so they are no longer seen. A faint vertical bar passing through the center is due to majority-spin $d_{x^2-y^2}$ emission and an “X” in the center of the image originates from the majority-spin d_{xy} initial state located 0.2 eV below E_F and observed due to our finite experimental resolution. All of the deductions of the symmetry of the initial states from photoemission selection rules are consistent with those from the calculations.

To quantify the dispersion of the electronic structure of the 1.2 ML film and further identify some of the features, additional images were taken at intermediate photon energies to those shown in Fig. 2. The

locations of the various structures in the images were tracked versus k_{\perp} along the [10] and [11] azimuths. These Fermi surface features are plotted in Fig. 3 along with Wang and Callaway's calculated bulk Ni Fermi surface [16].

The filled diamonds show the 3d-band FS crossings and the open circles show the location of the ringlike sp band which appears as a faint arc in the 45 eV images. The crosses show the location of a dispersionless peak located at the zone boundary, the most intense feature in the 90 eV image. This feature cannot be identified with a specific initial state without inclusion of multiple scattering analysis [15]. The open diamonds show the location of the d_{xy} initial states located 0.2 eV below E_F , not part of the Fermi surface, yet observed in our image.

From these observations, we conclude that the Ni exhibits bulklike electronic dispersion, even in films as thin as 1.2 ML, with the relative intensities and polarization dependences in good agreement with calculations.

This bulklike electronic structure can be understood if there is significant hybridization between the Ni film and the Cu substrate. The radial extent of the Ni 3d levels, such as the d_{xz} and d_{yz} , confines their interactions to nearest-neighbors and this interaction is strongly screened by the sp electrons. The sp states, however, extend to additional neighboring sites so that interface hybridization with the substrate will involve the Ni $sp-d_{z^2}$ hybrid and the Cu sp , both of which cross E_F . Through that hybridization, the Bloch periodicity of the substrate is imposed on the electronic wave functions in the film.

A tight binding study of the electronic structure of a Ni monolayer on Cu(001) illustrates the importance of hybridization effects at the interface [6]. Little difference was found between the dispersion of electronic states for the bulk Ni(001) surface layer and the one monolayer film of Ni/Cu(001). Depolarization of the Ni d band was found to occur by hybridization with the Cu sp band while the Cu 3d band was relatively unimportant. One might expect to observe a narrowing of the Ni 3d band due to a reduced coordination of the surface atoms with respect to the bulk. However, no narrowing is evident in the photon energy dependence of the emission from the "pure 3d" d_{xz} and d_{yz} orbitals, due to strong screening by the sp electrons.

This observation of hybridization of like 3d transition metals is not limited to this single system: We have observed similar behavior in atomically thin Cu/Ni(001) and Co/Cu(001) films. We attribute this to the similar electronic structures, differing primarily in band-fitting, and to the small lattice mismatch, $\sim 2.5\%$ for Ni/Cu(001). Recent calculations on Co/Cu superlattices [17] show that there is a strong hybridization between the Co d bands and the Cu sp bands. Co, however, has a lower band filling compared to Ni, so that the $sp-d_{z^2}$ band in Co lies above E_F . Thus the mechanism for hybridization in Co/Cu involves the Co d bands and the Cu sp bands. The higher band filling in Ni results in the Ni $sp-d_{z^2}$ hybrid

band being partially filled at E_F , facilitating hybridization with the Cu sp band.

The hybridization of the Ni $sp-d_{z^2}$ band with the Cu sp band plays a crucial role in determining the nature of the electronic structure of these films and yields a mechanism for the film to interact with the substrate crystal field. Through this interaction, a two-dimensional array of Ni atoms develops the characteristics of a bulk electronic structure giving rise to a complete three-dimensional Fermi surface. The strength of this interaction will determine the degree of bulklike versus two-dimensional electronic behavior in other thin film systems.

We would like to thank Dr. Z. Qu and the staff of the CAMD synchrotron for their important contributions to this study. This work was funded by the Louisiana Educational Quality Support Fund (1992-95)-RD-A-07 and by NSF under Grant No. DMR-9222646.

*Present address: Department of Physics, Center for Materials for Information Technology, University of Alabama, Tuscaloosa, AL.

- [1] J.E. Ortega and F.J. Himpsel, Phys. Rev. Lett. **69**, 844 (1992).
- [2] S.S.P. Parkin, R. Bhadra, and K.P. Roche, Phys. Rev. Lett. **66**, 2152 (1991).
- [3] J.M. Gallego, D. Lederman, S. Kim, and I.K. Schuller, Phys. Rev. Lett. **74**, 4515 (1995).
- [4] J.G. Tobin, S.W. Robey, L.E. Klebanoff, and D.A. Shirley, Phys. Rev. B **28**, 6169 (1983).
- [5] H. Huang, X.-Y. Zhu, and J. Hermanson, Phys. Rev. B **29**, 2270 (1984); D.-S. Wang, A. J. Freeman, and H. Krakauer, Phys. Rev. B **24**, 1126 (1981).
- [6] J. Tersoff and L.M. Falicov, Phys. Rev. B **26**, 6186 (1982).
- [7] D. Li, J. Pearson, and P.D. Johnson, Phys. Rev. B **51**, 7195 (1995).
- [8] G.J. Mankey, M.T. Kief, F. Huang, and R.F. Willis, J. Vac. Sci. Technol. A **11**, 2034 (1993).
- [9] R.L. Kurtz, S.W. Robey, L.T. Hudson, R.V. Smilgys, and R.L. Stockbauer, Nucl. Instrum. Methods Phys. Res., Sect. A **319**, 257 (1992).
- [10] J. Shen, J. Giergiel, and J. Kirschner, Phys. Rev. B **52**, 8454 (1995).
- [11] G.J. Mankey, K. Subramanian, R.L. Stockbauer, and R.L. Kurtz, in *Applications of Synchrotron Radiation Techniques to Materials Science III*, MRS Soc. Symp. Proc. No. 437, edited by L.J. Terminello, S.M. Mini, H. Ade, and D. Perry (Materials Research Society, Pittsburgh, 1996), p. 39.
- [12] K. Subramanian, G.J. Mankey, R.L. Stockbauer, and R.L. Kurtz (unpublished).
- [13] N.V. Smith, Phys. Rev. B **19**, 5019 (1979).
- [14] N.V. Smith, P. Thiry, and Y. Petroff, Phys. Rev. B **47**, 15476 (1993).
- [15] E.L. Shirley, L.J. Terminello, and F.J. Himpsel, Phys. Rev. B **53**, 10296 (1996).
- [16] C.S. Wang and J. Callaway, Phys. Rev. B **15**, 298 (1977).
- [17] J.L. Pérez-Díaz and M.C. Muñoz, Phys. Rev. Lett. **76**, 4967 (1996).